ASME Journal of Heat and Mass Transfer
Online journal at:
https://asmedigitalcollection.asme.org/heattransfer

In-Situ Measurement of Thermal Barrier Coating Properties Via Induction Phase Radiometry: Methodology Development

Shani Eitan
Turbomachinery and Heat Transfer Laboratory,
Faculty of Aerospace Engineering,
Technion–Israel institute of Technology,
Haifa 3200003, Israel
e-mail: shanieitan@campus.technion.ac.il

Simon Julius
Turbomachinery and Heat Transfer Laboratory,
Faculty of Aerospace Engineering,
Technion–Israel institute of Technology,
Haifa 3200003, Israel
e-mail: simonjulius@gmail.com

Beni Cukurel[1]
Turbomachinery and Heat Transfer Laboratory,
Faculty of Aerospace Engineering,
Technion–Israel institute of Technology,
Haifa 3200003, Israel
e-mail: beni@cukurel.org

This research introduces a new method for accurately measuring the thermal resistance of thermal barrier coatings (TBCs), as typically used in gas turbine engines. The proposed method involves periodic internal heat generation inside the airfoil in the vicinity of the TBC-alloy boundary using low-frequency modulated induction heating through a coil. The phase lag between the radiation flux emitted to the surroundings from the exposed side of the TBC and the recorded voltage input to the modulated induction coil is proportional to the thermal resistance (L^2/α) of the thin film. A simplified analytical model is developed to quantify the relationship between the lag as a function of the thermal resistance and induction modulation frequency. Numerical experiments are conducted to solve the full physics. Comparing the output with the simplified model, precision of 0.8% under ideal conditions can be observed. Moreover, the robustness of the methodology to recover properties is characterized by differing levels and types of noise levels, including Gaussian and constant-lag biases. For the relevant application, it is found that the suggested approach maintains a recovery error bound to range of 1–10%, dependent on input noise level.
[DOI: 10.1115/1.4064457]

Introduction

Material Characteristics. Gas turbines for propulsion and power generation applications operate at elevated temperatures to maximize power density and efficiency. To this end, in addition to improved alloy design, enhanced microstructures, and cooling, insulating thermal barrier coating (TBC) layers are deposited on top of metallic components. Their application areas include first- and second-stage turbine vanes, blades, augmenters, combustors, and burner can parts such as transition pieces and heat shields [1].

TBCs are complex, multifunctional thin films with low thermal conductivity, excellent fracture toughness, and a large thermal expansion coefficient compared to other oxides, which helps to alleviate thermal stress. In gas turbine applications, the TBC structure is double-layered and deposited on the exposed surfaces of nickel or cobalt-based super alloy engine components. The first layer, referred to as the bond coat, is a metallic film which aids in protecting the substrate material against oxidation and corrosion in addition to good adhesion to the thermally insulating ceramic secondary layer. A typical cross section of a TBC layer is depicted in Fig. 1, where the upper layer is the insulating ceramic layer, the lower part of the image depicts the superalloy material, and the thin bond coat is seen between them in a darker grayscale shade. Currently, the two main processes used in industrial deposition of TBCs are electron beam physical vapor deposition and plasma spraying [2].

TBCs are required to exhibit high melting point, phase stability, low thermal conductivity, and thermal expansion that matches with the metal substrate so as to endure the challenging gas-turbine thermo-mechanical environment. Due to its outstanding durability, a 100 μm to 2 mm thick layer of yttria-stabilized zirconia (YSZ) in its metastable tetragonal-prime structure is the prime TBC choice

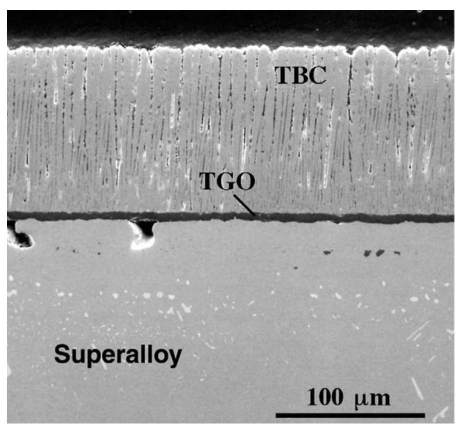

Fig. 1 Cross sectional image of a ceramic thermal barrier coating deposited via electron-beam evaporation on a superalloy, reproduced from Ref. [5] (Creative Commons Attribution CC BY-NC-ND 3.0 DEED @ 2005)

[1]Corresponding author.
Contributed by the Heat Transfer Division of ASME for publication in the Journal of Heat and Mass Transfer. Manuscript received July 16, 2023; final manuscript received December 25, 2023; published online February 7, 2024. Assoc. Editor: Anil Tolpadi.

for modern gas turbine blades [3]. With a typical Y_2O_3 weight percentage of 7–8% within ZrO_2, the diffusivity of YSZ is reported in the $3.6 - 5.6 \times 10^{-7}$ m^2/s range, while the thermal conduction coefficient is $0.42 - 0.98$ W/m K [4]. The thermal resistance parameter, L^2/α, reflects the structure's ability to act as a barrier between the harsh environment within the engine hot section and the blade material and should be maximized [5].

Thermal Barrier Coating Deterioration. In a typical operational environment experienced by TBCs, several factors contribute to the reduction of overall service life. Firstly, YSZ coatings are susceptible to a phase transition, which occurs at around 1470 K, where the metastable t′-phase transforms to t-phase, which transitions to a cubic and monoclinic phase during subsequent cooling [6]. This change in the crystalline structure greatly increases the sinter activity of YSZ, leading to reduced fracture toughness. Secondly, environmental dust erosion is a major contributor to TBC layer degradation as it causes material abrasion and simultaneously degrades thermal properties due to particle ingestion [7]. The erosion is then followed by infiltration of calcium-magnesium-alumina-silicate (CMAS) that originates in dust deposits, which leads to a rise in thermal conductivity and diffusivity, as well as volumetric heat capacity due to media fraction and distribution variations [8].

Considering these factors, TBCs must be routinely inspected to ensure that they fulfill their function. Inspections are required to avoid engine availability issues caused by high unscheduled engine removal rates. To address this issue, there is a need for in situ assessment of TBC thermo-mechanical properties.

Existing Thin Film Thermal Resistance Measurement Methodologies. Existing TBC thermal performance measurement techniques involve energetic excitation of the external surface of the component of interest. The temperature response is subsequently measured on the frontal or the back plane, depending on the technique. The thermal properties of the sample can be assessed through the solution to the one-dimensional heat conduction problem. It is commonly assumed that a sample composition is homogeneous and isotropic. The existing methods can be divided into three different categories, depending on their boundary condition and excitation types.

Constant excitation source techniques, such as the thin film thermal conduction meter (TFTCM) [9], require a dedicated setup with controlled environment to provide prescribed heat transfer conditions of constant heat flux on one side, and a heat sink on the other. Absent of significant lateral heat conduction losses or radiation heat exchange, the effective thermal conductivity can be measured through observations of cross-sectional temperature evolution. Although high measurement accuracy within $\pm 5\%$ can be achieved through such an approach, the methodology intrinsically precludes in situ inspection applications.

The second category incorporates a temporal change in heat flux boundary conditions. The laser flash [4] and pulsed thermal imaging multilayer analysis (PTI-MLA) [10] techniques are based on transient step forcing functions of the external surface, followed by temperature evolution measurement of the same surface through thermography or pyrometry. Although this approach is theoretically suitable for in situ measurements and can provide accurate results, it requires an extensive calibration and controlled environment due to reliance on the magnitude of the temperature response.

The third category is a natural extension of the two prior approaches which include measurement procedures that implement periodic transient forcing. In this case, the relevant TBC parameters can be deduced from the phase difference between the input and the output signals, or from frequency characteristics, negating the need for calibration. The most well-known of these methods is the 3-Omega technique [4], which uses a thin metal strip that is fabricated on top of the ceramic layer to create an excitation and measure the resulting response. Another approach is the photo-acoustic technique (PAT), which resolves the properties of thin film layers based on the evaluation of a photo-acoustic signal, which is generated at the solid–gas interface as a result of laser irradiation [11]. Both schemes are not suitable for in situ implementation, since 3-Omega requires on-surface addition of heat flux source, while PATs experimental complexity limits the technique to a laboratory setting and restricts its applicability to very thin samples (substrates with thickness below 2.5 mm and TBC with thickness below 50 μm).

The most advanced periodically excited methods are the Phase of photothermal emission analysis (PopTea) [12] and the thermal wave interferometry (TWI) techniques [13]. Both approaches use different methods to determine material properties while both require the phase lag between input irradiation and output emission to be known so as to derive the material's thermal properties. While PopTea is based on solving transient heat transfer equations with a linear radiation transport model to acquire an expression for phase, TWI implements a more simplified term for the phase by assuming independency of radiative parameters and applying a sensitivity analysis. Due to the inherent nature of the 2-layer model solution that PopTea resolves, which contains an input signal passing through both layers, it produces results with relatively high inaccuracy (20%). Additionally, the invasive radiative measurement approach

Table 1 Summary of state-of-the-art thin-film thermal property evaluation methods

Method	Description	Accuracy	In-situ capability and limitations
Steady-state boundary conditions methods			
TFTCM	Isolated specimen with heat flux source at its bottom	5%	Not in-situ capable. Requires vacuum, antiradiant cell
Step change boundary conditions methods			
Laser flash	Temperature response due to laser pulse source	20%	Not in-situ capable. Requires vacuum/inert cell
PTI-MLA	Temperature response due to flash lamp pulse	2%	Low in-situ capability Requires enhanced emissivity coating, IR calibration, and special optical equipment
Periodic excitation boundary conditions methods			
3-Omega	Temperature response due to AC electrical heating element	1–5%	Not in-situ capable Requires wire strapping
Photo-acoustic	Measurement of acoustic waves created by fluctuating heat generated via laser	10%	Not in-situ capable Requires closed cell
PopTea	Phase of photothermal emission, created by laser heating	20%	Requires an elliptical mirror, variable beam aperture, signal modulator, CO_2 laser, and an IR detector
TWI	Phase of thermal waves from TBC-substrate interface interference	3–6%	Not in-situ capable. Requires enhanced emissivity coating. Requires same optical equipment as in PopTea

requires complex equipment including an elliptical mirror, variable beam aperture, signal modulator, CO_2 laser, and an IR detector, and is therefore not suitable for in situ gas-turbine inspection.

Moreover, methods that rely on a periodic excitation and subsequent phase lag are incapable of decoupling sample thickness from thermal properties. Instead, the thermal resistance analogy is applied to quantify the state of the sample in question. When performing heat conduction analysis, a common measure for the ability to resist the temperature rise (ΔT) due to heat flux (Q) is thermal resistance ($R_n = \Delta T/Q$). For rectangular slabs, the thermal resistance is defined as, $R_n = L/kA$, where L is the plane thickness, A is its area, and k is the thermal conductivity. This formulation can also be described in terms of diffusivity to take the form of

$$R_n = \frac{L^2}{\alpha mc} = \frac{L^2}{\alpha} \cdot \frac{1}{C} \tag{1}$$

where α is the thermal diffusivity, m is the mass, c is the specific heat capacity, and C is the heat capacity ($C = c \cdot m$). Since infiltration of amorphous CMAS changes the volumetric heat capacity marginally, it can be considered a constant dependent on the TBC composition and deposition methods, but largely invariant during the operational life [8]. Then, monitoring of the ratio value $R = R_n C = L^2/\alpha$ provides a good indicator of proportional deviations in TBC thermal performance [12] from a reference state when C can be known.

The accuracies and in situ measurement capabilities of the techniques are summarized in Table 1. The methods themselves and relevant investigations are further described in Appendix A. It can be concluded that due to various complexities associated with the current state-of-the-art measurement techniques, there is no available methodology that would allow a sufficiently accurate and in situ measurement of TBC thermal performance directly on installed turbine environments.

Motivation and Proposed Approach

Since thermal barrier coatings are developed to provide sustained thermal protection for engine components, a reliable, nonintrusive, and quantitative measurement that would assess the layer's thermophysical properties and microstructure (and thus determine the coatings performance) is in high demand. In-situ health monitoring of TBC performance (without removing it from the engine) could lead to considerable cost savings and safety improvements. However, measurement of the thermal resistivity for thin ceramic coatings remains to be one of the more complicated problems. In this light, this paper aims to present a new in situ, high-accuracy, and calibration-free measurement technique that attempts to address this critical gap.

In our approach, a high-frequency carrier signal (in the order of 100 kHz), is modulated by a low-frequency wavelength (of approximately 1 Hz) in order to produce periodic inductive heating near the metal boundary of a TBC coating. To accurately measure the phase difference between the excitation and thermal response, the necessary experimental equipment consists of a function generator with signal modulation capabilities, an induction amplifier, a coil, and a sampling pyrometer with a measurement frequency in the kHz range. Then, the time series associated with the voltage input to the coil and the pyrometer output proportional to the radiation flux are simultaneously recorded using a data acquisition device and sampled across a range of sweep frequencies. In the frequency domain, the resulting useful information is the phase of the radiation flux with respect to the coil's low-frequency modulation signal varied across a predetermined range. Then, the thermal resistance of the coating can be found by minimizing the error between the analytical model and the phase measurements in a weighted least squares scheme.

Considering that the proposed technique does not rely on magnitude of the temperature response, the need for emissivity calibration and controlled environment is eliminated. Moreover, the thermal resistance of the thin coating is resolved with a high accuracy since heat is generated internally, as opposed to all other techniques which require energy transfer through the ceramic. In-situ capability is obtained, as there is no need for a controlled environment.

Recovery Method Development

Induction Heating. A periodically varying voltage applied to a wire results in an alternating current (AC) flow. In turn, a time-varying magnetic field is produced, which induces eddy currents in electrically conductive objects located in its vicinity. Although there are many types and shapes of inductors, the most common one is the solenoid multiturn coil, Fig. 2. Then, the distribution of electrical field lines can be determined via Maxwell equations with the quasi-steady approximation [14]. These induced currents have a frequency equal to that of the coil current and produce heat via the Joule effect. This phenomenon is known as induction heating [15].

In the scope of the current research, the internal heat generation is introduced into the parent material layer, which is the super-alloy substrate. The power P is thermalized in accordance with Joule's law

$$P = I^2 R_{\mathrm{el}} \tag{2}$$

where I and R_{el} are eddy current and electrical resistance, respectively. In the high-frequency limit, the current distribution and resulting thermalization become concentrated near the surface of the substrate, commonly known as the skin effect.

Then, the spatial current density distribution I along the workpiece thickness from the interface boundary x, can be represented by the following [15]:

$$I(x) = I_0 e^{-x/\delta} \tag{3}$$

where I_0 is the surface current density (A/m^3). The penetration depth, δ, which contains approximately 86% of the power, can be evaluated using [15]

$$\delta = 503\sqrt{\frac{\rho_{\mathrm{el}}}{\mu_r f_c}} \tag{4}$$

where f_c is the carrier frequency of the electromagnetic field Hz, μ_r is the relative permeability, and ρ_{el} is the electrical resistivity of the material. In a simple rectangular conductor, the relation between resistivity (ρ_{el}) and resistance (R_{el}) is

$$R_{\mathrm{el}} = \frac{\rho_{\mathrm{el}} l}{A_c} \tag{5}$$

where l is the length of the conductor and A_c is its cross-sectional area. Through substitution, the spatial term of the heat generation density function (W/m^3) can be found as

$$g(x) = R_{\mathrm{el}} I(x)^2 = \frac{\rho_{\mathrm{el}} l}{A_c} I_0^2 e^{-2x/\left[503\sqrt{\frac{\rho_{\mathrm{el}}}{\mu_r f_c}}\right]} \tag{6}$$

In following, the 1-D heat conduction problem with internal generation term can be solved for a semi-infinite slab made of

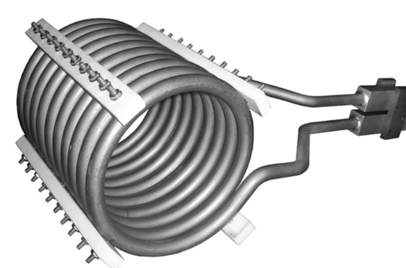

Fig. 2 Multiturn solenoid inductor coil [15]

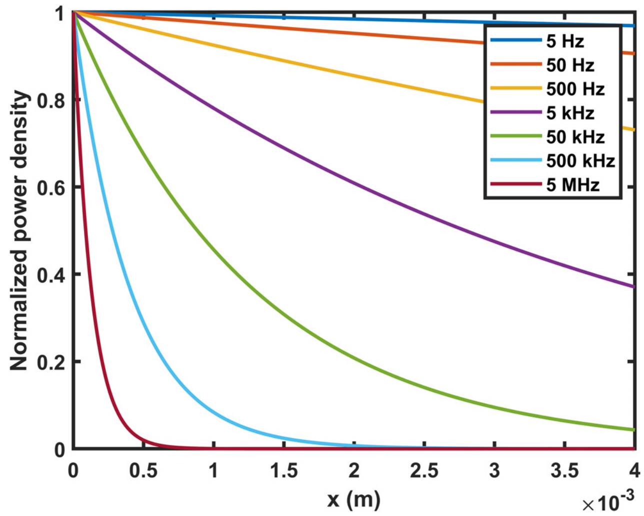

Fig. 3 Power density distribution (Skin effect) inside 4[mm] Inconel 625 sample for different frequencies normalized by $R \cdot I^2$

Inconel 625 (with a relative permeability of 1.006 and resistivity $1.29\,\mu\Omega \cdot \mathrm{m}$), see Ref. [16] for full solution. Figure 3 portrays the power density distribution for different excitation frequencies. At the high-frequency limit, most of the heating occurs near the edge of the substrate. Therefore, a carrier frequency (f_c) of $\mathcal{O}(10^5\,\mathrm{Hz})$ is used to create the induction process. While such frequencies are vital for the internal generation, the diffusive characteristics of Fourier heat conduction processes decay these oscillations across short time and length scales. Then, in order to study the response of the thin ceramic film attached, the carrier signal must be modulated at a significantly lower frequency f_m of $\mathcal{O}(1\,\mathrm{Hz})$.

Model Solution of Phase Response. Consider a two-layer slab comprised of a ceramic coating and a metallic substrate layer subject to induction heating with a conducive carrier frequency, Fig. 4. The phase-lag solution from the electrical source to the temperature at the TBC boundary is broken down into a series of consecutive transfer functions that represent induction heating, diffusion across the substrate to the backside of the TBC coating, and the conduction process across the TBC coating to the exposed surface (summarized in Fig. 5). Note that phase lag may also be dependent on the properties of the bond coat, that usually exists in TBC deposition. However, the phase-lag contribution is undoubtedly small given typical thickness of bond coats; therefore, its effect is neglected in the scope of this paper.

Due to the extremely low efficiency of induction heating at the modulation frequency (1 Hz), the carrier frequency is solely responsible for the thermalization of the electrical energy into internal generation. The modulation frequency simply acts as a time-varying gain on the generation power itself. Therefore, a modulated form of the internal generation Joule heating term is derived from

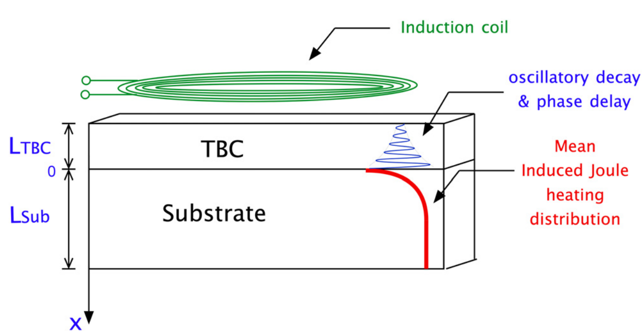

Fig. 4 Schematic of the induction heating and associated diffusion problem

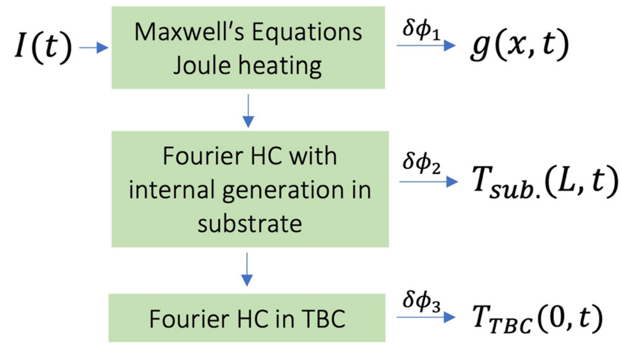

Fig. 5 Breakdown of the induction heating and diffusion problem into a series of consecutive transfer functions, each with a phase-lag contribution

Maxwells equations. Consider an induction coil that is being supplied by an alternating current of amplitude I_0, carrier frequency ω_c. The electric field from the coil surface boundary is described as

$$E = E_0 \cos(\omega_c t) \tag{7}$$

where E is the electrical field time distribution and E_0 is its amplitude. The current density field established within the conductive substrate material is described by, assuming the displacement current is negligible

$$I = \sigma E \tag{8}$$

The solution to a current oscillation inside a good conductor induced by a coil's electromagnetic field is derived from Maxwell's equations describe the current within the conductor [17]

$$I(x) = \sigma E_0 e^{-(x+d)\sqrt{\frac{\omega_c \mu \sigma}{2}}} \cos\left(\omega_c t - (x+d)\sqrt{\frac{\omega_c \mu \sigma}{2}}\right) \tag{9}$$

where the skin depth is defined as $\delta = \sqrt{2/\omega_c \mu \sigma}$, which is equivalent to the common term introduced earlier, and d is the distance from the induction coil to the substrate material

$$I(x) = \sigma E_0 e^{-\frac{x+d}{\delta}} \cos\left(\omega_c t - \frac{x+d}{\delta}\right) \tag{10}$$

The internal heat generation distribution is

$$g(x,t) = I_x^2 R_s = \frac{\sigma^2 E_0^2 R_s}{2}\left[1 + \cos\left(2\omega_c t - \frac{2(x+d)}{\delta}\right)\right] e^{-\frac{2(x+d)}{\delta}} \tag{11}$$

When the induction is modulated at frequencies that do not induce a significant electromagnetic field in the substrate, considering that the timescales between carrier and modulation frequencies are several orders of magnitude apart, this modulation can be applied directly on the generation term

$$g(x,t) = \frac{\sigma^2 E_0^2 R_s}{4}\left[1 + \cos\left(2\omega_c t - \frac{2(x+d)}{\delta}\right)\right](1 + \cos(\omega_m t))\, e^{-\frac{2(x+d)}{\delta}} \tag{12}$$

where R_s is the effective substrate resistance, μ is the magnetic permeability, σ is the electrical conductivity and ω_m is the modulation frequency. (In real application, note that the generation is also dependent on the coil standoff distance, surface curvature, and other geometrical complexities, which may create limitations for this technique.) Depicted in Fig. 6, the generation term is considered for a typical substrate thickness of a turbine blade L_{sub}=4 mm, i.e., for the range of $x = [0, L_{\mathrm{sub}}]$.

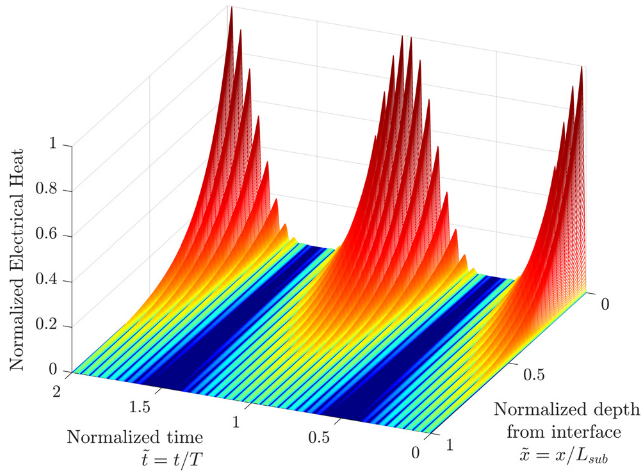

Fig. 6 Normalized substrate internal generation distribution for a typical turbine superalloy

To obtain the transfer function that relates the TBC-substrate interface temperature to the input current signal, the following 1D nonhomogeneous Fourier heat conduction boundary value problem is to be solved for the substrate

$$T_{x=L_{\rm sub}} = 0,\ k\frac{\partial T}{\partial x}_{x=0} + hT_{x=0} = 0;\quad \frac{1}{\alpha}\frac{\partial T}{\partial t} = \frac{\partial^2 T}{\partial^2 x} + \frac{g(x,t)}{k} \tag{13}$$

The boundary condition $T = 0$ at $x = L_{\rm sub}$, represents a shifted fixed temperature, adapted for convenience and generality of the solution. The boundary condition at $x = 0$ simply assumes a conduction of heat proportional to the temperature at the interface. Although the more precise approach is to solve the multislab problem and obtain a solution that can then be inter-rogated between the slab layers to obtain the local phase-lag, this would preclude a physically insightful breakdown of the various transfer functions that make up the phase-lag. Nevertheless, it is observed that the phase-lag solution is insensitive to the precise boundary condition and a direct result of the internal generation distribution. In the following, substituting for the generation term (Eq. (12)), the phase lag solution is obtained.

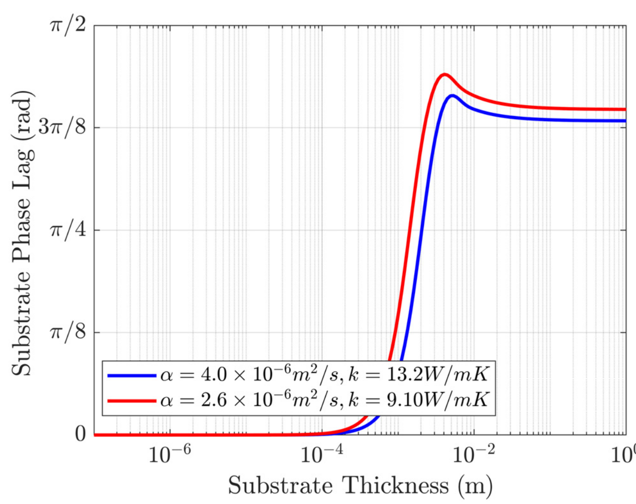

Fig. 7 Phase lag between TBC-substrate interface and input modulation signal ($\delta\phi_1 + \delta\phi_2$) with varying substrate thickness for max and min Inconel properties, f_c=100,000 Hz, f_m=1 Hz

For typical excitation frequencies, Fig. 7 shows the envelope of phase variation as a function of substrate thickness for the bounds of Inconel conductivities and diffusivities. Considering the two different diffusivity properties, the phase relation is nearly identical for substrate thicknesses less than 5 mm. At substrate scales of 10^{-4} m, the thin layer assumption holds, and the phase lag converges to zero. In the large thickness limit, the phase lag reaches a maximum value of around $\frac{3\pi}{8}$. Typically, the geometry and properties of the inner core structure of the turbine blade are well known, thus allowing for the exact lag contribution to be estimated when necessary.

For the final transfer function, the nonhomogeneous forcing Dirichlet boundary condition is considered at the interface of a one-layer TBC slab. However, this approach clearly does not consider the effects of curvature and multidimensional conduction in the specimen, where the one-dimensional heat conduction assumption might not hold.

Consider a single TBC layer with a nonhomogeneous boundary condition on the backside representing Joule electrical heat generation and homogeneous Robin boundary condition on the front side, representing conductive and convective heat losses. Radiative heat losses can be safely ignored as mean temperature and its variations are anticipated to be small. The heat transfer problem is described as follows:

$$T_{x=0} = f(t);\quad \frac{\partial T}{\partial t} = \alpha\frac{\partial^2 T}{\partial^2 x};\ k\frac{\partial T}{\partial x}_{x=L} + hT_{x=L} = 0 \tag{14}$$

where T denotes the temperature, $\alpha = k/\rho C_p$ is the thermal diffusivity, $f(t)$ is a time-dependent surface generation term at the coating-substrate interface and h is the convective heat transfer coefficient at the exposed side of the TBC layer. Note that there is no heat generation term within the TBC, as it is manifested in the nonhomogeneous boundary condition at $x = 0$. We are interested in describing a transfer function for the evolution of the temperature field between $x = 0$ and $x = $L, where L is the TBC thickness. The transfer function will enable us to operate on the input to get the phase of the output. For this, we can simply solve the equation in frequency space (applying a Laplace transform)

$$\mathcal{L}(T(x,t)) = \bar{T}(s,x) = \int_0^\infty T(x,t)e^{-st}dt \tag{15}$$

The equations become

$$\bar{T}_{x=0} = f(s);\ s\bar{T} = \alpha\frac{d^2\bar{T}}{dx^2};\quad k\frac{d\bar{T}}{dx}_{x=L} + h\bar{T}_{x=L} = 0 \tag{16}$$

Solving for the boundary conditions yields

$$\bar{T}(\mathrm{s},\mathrm{x}) = \frac{\bar{\mathrm{f}}(\mathrm{s})\left(e^{-\sqrt{\frac{s}{\alpha}}x} + e^{\sqrt{\frac{s}{\alpha}}(\mathrm{x}-2L)}\left(\frac{k\sqrt{\frac{s}{\alpha}}-h}{k\sqrt{\frac{s}{\alpha}}+h}\right)\right)}{1 + e^{-2\sqrt{\frac{s}{\alpha}}L}\left(\frac{k\sqrt{\frac{s}{\alpha}}-h}{k\sqrt{\frac{s}{\alpha}}+h}\right)} \tag{17}$$

In order to prepare a transfer function, the function in $x = $L and in $x = 0$ is calculated

$$\bar{T}(s,0) = \bar{f}(s) \tag{18}$$

$$\bar{T}(\mathrm{s,L}) = \frac{\bar{\mathrm{f}}(\mathrm{s}) e^{\sqrt{\frac{s}{\alpha}}L} 2k\sqrt{\frac{s}{\alpha}}}{e^{2\sqrt{\frac{s}{\alpha}}L}\left(k\sqrt{\frac{s}{\alpha}}+h\right)+\left(k\sqrt{\frac{s}{\alpha}}-h\right)} \tag{19}$$

By definition, the transfer function is the ratio between the output and input

$$H(s) = \frac{\bar{T}(\mathrm{s,L})}{\bar{T}(\mathrm{s},0)} = \frac{2e^{\sqrt{\frac{s}{\alpha}}L}}{\left(e^{2\sqrt{\frac{s}{\alpha}}L}+1\right)+\left(\frac{h}{k}\sqrt{\frac{\alpha}{s}}\right)\left(e^{2\sqrt{\frac{s}{\alpha}}L}-1\right)} \tag{20}$$

Rearranging the transfer function to a more convenient expression and setting $s = i\omega$

$$H(i\omega) = \frac{1}{\cos((1-i)W_o) + \frac{(1+i)}{2}\frac{B_i}{W_o}\sin((1-i)W_o)} \tag{21}$$

where $B_i = hL/k$ is the Biot number and $W_o = \sqrt{\omega L^2/2\alpha}$, alludes to the Womersley number. The W_o nondimensional parameter represents the ratio between the pulsatile thermal forcing and the retarding effect of heat diffusion. Then, the phase of the transfer function is defined as:

$$\delta\phi_3 = \tan^{-1}\left[\frac{Im(H(i\omega))}{\mathrm{Re}(H(i\omega))}\right] + \phi_\Delta \tag{22}$$

where

$$\phi_\Delta = \pi \cdot \min\left\{\frac{\mathrm{Re}(H(i\omega))}{|\mathrm{Re}(H(i\omega))|}, 0\right\} \tag{23}$$

This gives

$$\delta\phi_3 = \tan^{-1}\left[\frac{\frac{Bi}{2W_o}\left[\begin{matrix}-\sin(W_o)+\\ \cos(W_o)\tanh(W_o)\end{matrix}\right] - \sin(W_o)\tanh(W_o)}{\frac{Bi}{2W_o}\left[\begin{matrix}\sin(W_o)+\\ \cos(W_o)\tanh(W_o)\end{matrix}\right] + \cos(W_o)}\right] + \phi_\Delta \tag{24}$$

Several observations can be drawn from Eq. (23). If Biot number is sufficiently large, $\mathcal{O}(B_i/2W_o) \gg 1$, or small $\mathcal{O}(B_i/2W_o) \ll 1$, the equation is reduced to a form that has no Biot number dependency

$$B_i/2W_o \gg 1 \rightarrow \\ \delta\phi_3 \approx \tan^{-1}\left[\frac{-\tan(W_o)+\tanh(W_o)}{\tan(W_o)+\tanh(W_o)}\right] + \phi_\Delta \tag{25}$$

$$B_i/2W_o \ll 1 \rightarrow \\ \delta\phi_3 \approx \tan^{-1}[-\tan(W_o)\tanh(W_o)] + \phi_\Delta \tag{26}$$

Independent decoupling of L and α from the prescribed frequency and the measured phase response requires the phase angle to be a function of both Bi and W_o and is therefore impossible for the low and high Biot number limits. Instead, L and α can only be recovered when B_i is of $\mathcal{O}(1)$, however, since the TBC thickness is typically of the $\mathcal{O}(10^{-4}\,\mathrm{m})$ and its thermal conductivity is of $\mathcal{O}(1\,\mathrm{W/mK})$, this Biot number condition can only be satisfied when the heat transfer coefficient becomes sufficiently high (h is of $\mathcal{O}(10^4\,\mathrm{W/m^2K})$ or when using very low modulation frequencies of $\mathcal{O}(10^{-2}\,\mathrm{Hz})$. This observation renders direct decoupling of L and α impractical and necessitates a different approach.

Hence, the figure of merit for performance/health monitoring used in this work is thermal resistance, $R = L^2/\alpha$, which simultaneously relies on the TBC thickness and its thermal diffusivity while increasing as a response to both conducive trends (thicker layers or coatings with lower thermal diffusivity). In addition, this value does not rely on Biot number, and since excitation frequency is a known parameter, L^2/α can be recovered directly from W_o. In the case of the present effort, B_i is of $\mathcal{O}(10^{-4})$ and thus reduced formulation derived in Eq. (26) can be implemented to evaluate W_o from the phase angle.

Limits on Modulation Frequencies Band. There are practical limits that define the acceptable ranges of modulation frequencies for the tested sample, which are affected by several considerations. The first consideration is a consequence of periodicity of the phase response, Fig. 8. The W_o range should be anticipated to ensure that there is a one-to-one mapping to the measured phase lag. This can be achieved by ensuring a frequency range that yields a W_o value that does not exceed π. An additional constraint to the upper bound measurement is related to the magnitude of heat transfer function, Fig. 9. For all Biot numbers, it can be observed that the active bandwidth, for which the magnitude of the thermal variations is halved, occurs at a Womersley number of $\pi/2$, and a 90% signal drop occurs around a Womersley number of π. Therefore, we shall impose $W_o < \pi/2$ to ensure a sufficiently strong output signal.

Additionally, the critical consideration for the optimal modulation frequency is to ensure that there is a high degree of phase variation for small perturbations in Womersley number. To this end, a sensitivity analysis is conducted on the closed-form solution for phase (Eq. (26)) at small Biot numbers to determine the bounds of W_o. The derivative $\partial\delta\phi_3/\partial W_O$ is

$$\frac{\partial\delta\phi_3}{\partial Wo} = -\frac{\left(1+\tan^2(Wo)\right)\tanh(Wo) + \tan(Wo)\left(1-\tanh^2(Wo)\right)}{\tan^2(Wo)\tanh^2(Wo)+1} \tag{27}$$

This equation has a minimum at $W_o = 0$, an inflection point at $W_o \cong 3\pi/8$, and a linear dependency $\left(\frac{\partial\delta\phi_3}{\partial Wo} = 1\right)$ for $W_o > 3\pi/4$, Fig. 10. The frequency measurement lower bound can be determined according to desired phase variation detectability. It is suggested that a phase-Wo sensitivity greater than 0.2 is satisfactory, which corresponds to a minimum Womersley Number of 0.1.

An additional consideration for in situ experiment is the selection of the frequency lower bound to be determined by the desired time period for the induction heating procedure. Estimating that a cycle of up to 10 s is acceptable, a frequency in the range of 0.1 Hz would be

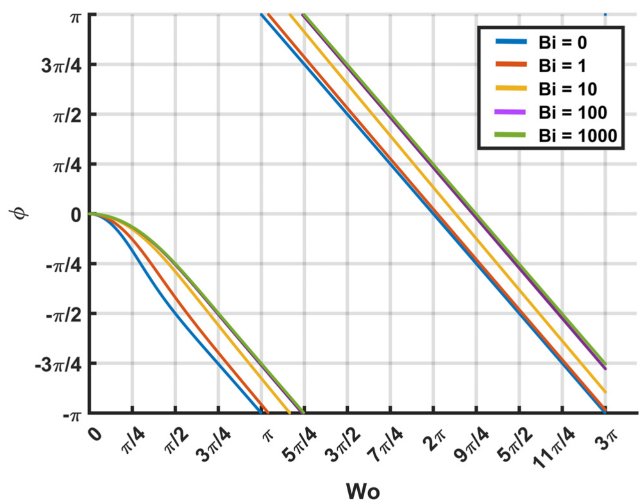

Fig. 8 Relationship between transfer function phase ($\delta\phi_3$) and thermal Womersley number for various Biot numbers at the free surface

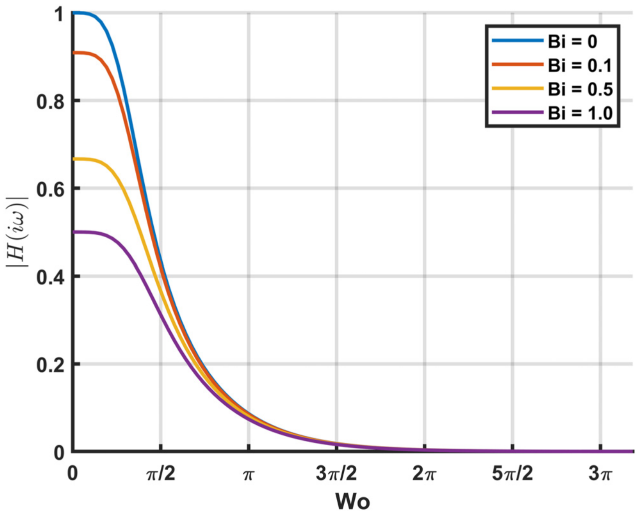

Fig. 9 Relationship between transfer function magnitude $|H(i\omega)|$ and thermal Womersley number for various Biot numbers at the free surface

required. Typical thicknesses and diffusivities of TBCs provide an approximate Womersley number

$$W_o = \sqrt{\frac{\omega L^2}{2\alpha}} \sim \frac{1}{2}\sqrt{\omega} \tag{28}$$

Thus, taking all these considerations into account, the Womersley number and corresponding modulation frequency range is established as

$$\begin{aligned} \frac{2}{5} &< W_o < \frac{\pi}{2} \\ 0.1\text{Hz} &< f_m < \frac{\pi}{2}\text{Hz} \end{aligned} \tag{29}$$

In practice, due to the presence of measurement noise, multiple observations should be conducted to reduce uncertainties.

Phase Measurement Results and Analysis

Thermal Property Recovery Under Ideal Conditions. In an experimental setting, the baseline experimental apparatus must include a function generator with signal modulation capabilities, an induction amplifier, a coil, and a sampling pyrometer with measurement frequency of the kHz order to ensure a high resolution of the phase shift. A voltage data acquisition device can be used to store the voltage input to the coil and the radiation flux proportional pyrometer output simultaneously. The data is collected by sweeping across a predefined range of frequencies. The recorded signal includes the time series of the pyrometer's radiation flux reading and the phase of this reading in the frequency domain, relative to the low-frequency modulation signal imposed on the induction coil. Given a collection of frequency-domain experimental data across relative phase shift and frequency pairs (ϕ, ω), finding the thermal resistance will require solving for $R = L^2/\alpha$ on a best-fit basis.

In the scope of the present work, numerical experiments are conducted. The physics of the problem are generated using the full analytical phase expression (Eqs. (21) and (22)), which captures the real heat conduction phenomena, absent of any assumptions

$$\delta\phi_3 = f\left(\vec{\omega}, \vec{R}, Bi\right) \tag{30}$$

For any given thermal resistance R, Fig. 11 illustrates the resultant relationship between the phase angle ϕ, and modulation frequency ω at typical $\mathrm{Bi} = 5 \times 10^{-4}$. This is the information that is captured by the pyrometer phase in reference to the induction coil modulation signal and represents the ideal measurement conducted for any thermal resistance value.

Then, the model is used to approximate the phase content for a range of frequencies, which are described by the reduced Eq. (26), providing

$$\phi_r = f\left(\vec{\omega}, \vec{R}\right) \tag{31}$$

Let us consider a typical TBC, with a thickness L of 5×10^{-4} m, and thermal diffusivity α of 4×10^{-7} m^2/s, yielding a thermal resistance value of $R_o = 0.625$ s. In following, controlling our induction coil, we should conduct a modulation frequency sweep across [0 2] Hz. Then, an error function $\Delta\phi$ can be defined to quantify the difference between the experiments, and the model φ_r such that it is wrapped in the interval $[-\pi, \pi]$

$$\Delta\phi\left(\vec{\omega}, R\right) = \pi - \left|\left|\delta\phi_3\left(\vec{\omega}, R_o, Bi\right) - \varphi_r\left(\omega, \vec{R}\right)\right| - \pi\right| \tag{32}$$

Figure 12 depicts a graphical representation of the absolute average error across all frequencies $\left|\overline{\Delta\phi}\left(\vec{R}\right)\right|$. The minimum value of the expression $\min\left|\overline{\Delta\phi}\right|$ leads to the correct retrieval R_r of prescribed R_o

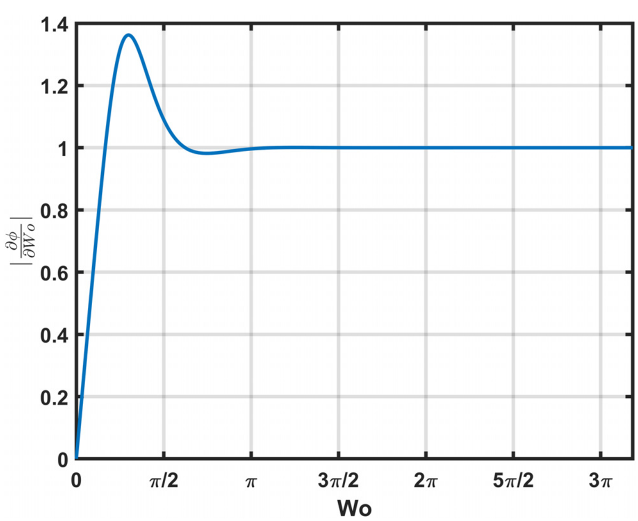

Fig. 10 Sensitivity of phase variation ($\partial\delta\phi_3/\partial Wo$) for small Biot numbers

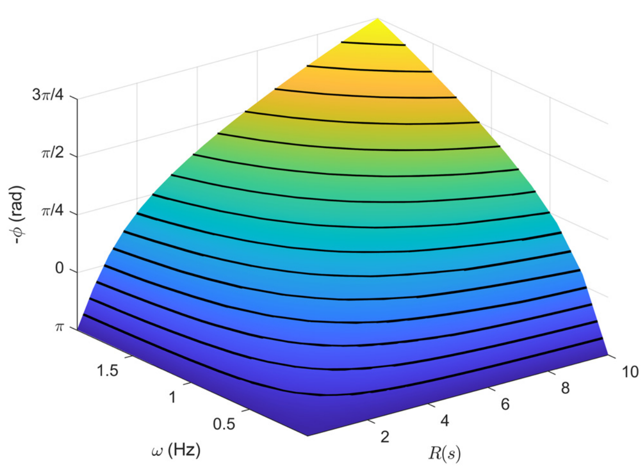

Fig. 11 Relationship of phase angle $\delta\phi_3$, with respect to modulation frequency ω and thermal resistance R at typical $\mathrm{Bi} = 5 \times 10^{-4}$

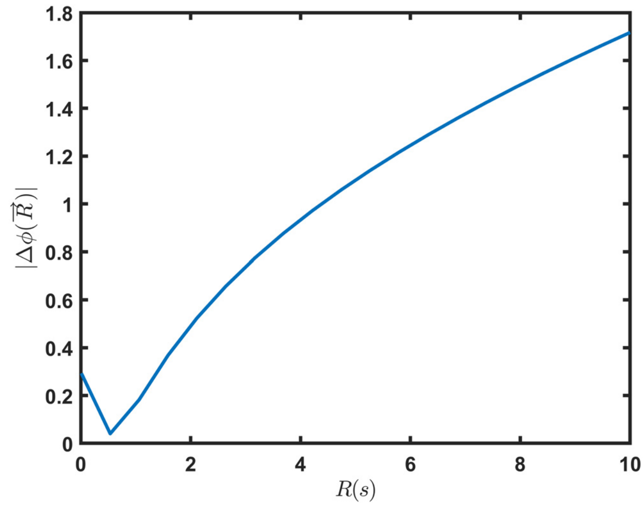

Fig. 12 Recovery of thermal resistance R from minimization of phase angle error function for nominal synthetic specimen with properties $L = 5 \times 10^{-4}$ m, $\alpha = 4 \times 10^{-7}$ m^2/s, at typical Bi $= 5 \times 10^{-4}$

and is obtained through implementation of the 'fminsearch' optimization algorithm in Matlab.

Expanding these measurements for a range of TBC samples with R_o [0.01×10] s under Bi [$10^{-5} \times 0.01$], (derived from h/k range [0.1×10] m^{-1}, L range [$10^{-4} \times 10^{-3}$] m, α range [$10^{-7} \times 10^{-6}$] m^2/s), Fig. 13 presents the error in R_o recovery under ideal conditions. For all scenarios, the maximum error observed is 0.8%, occurring at the high Biot numbers and low thermal resistances.

Sensitivity to Measurement Noise

To assess the robustness of the property recovery method, noise is introduced into the governing parameters. The first type of noise considered is on the modulation frequency due to an uncertainty in the induction amplifier system dynamics. The probabilistic nature of experimental apparatus is assumed to have a Gaussian probability distribution function

$$\begin{aligned} \omega_n &= \omega_s + \omega' \\ \omega' &\sim N(0, \sigma_\omega) \end{aligned} \tag{33}$$

where ω_s is desired frequency set value, σ_ω is standard deviation representing the level of frequency noise, and ω_n is the resulting

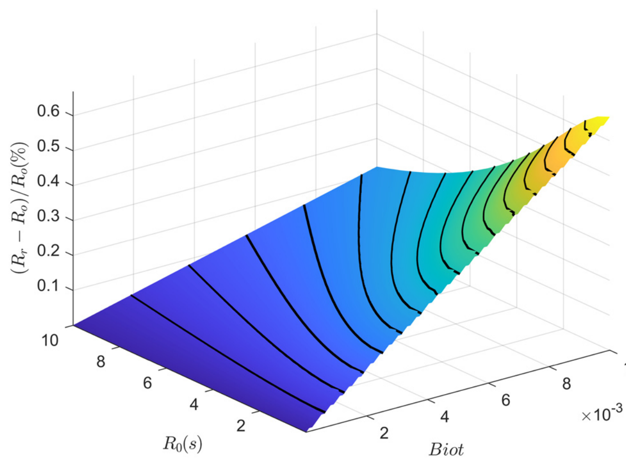

Fig. 13 Normalized percent error in recovery of sample thermal resistance R_o for range of specimens with different R and Biot values

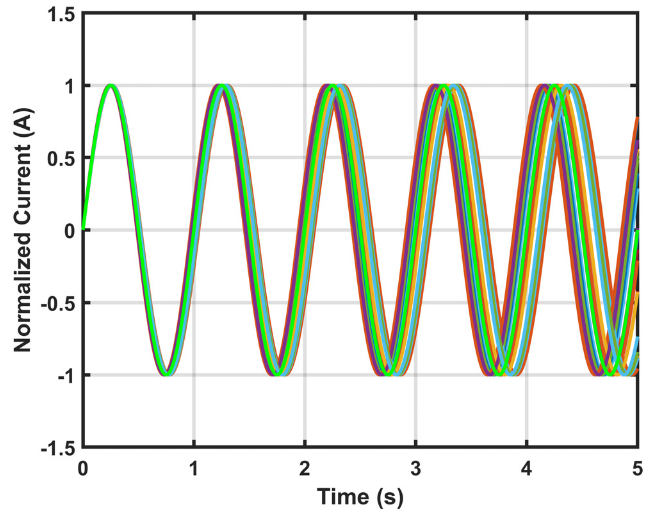

Fig. 14 An exemplary current output signal from the induction coil amplifier with deviations from intended frequency of $\omega_s = 1$ (Hz) and $\sigma_\omega = 2\%$, where the ideal signal is depicted in bright color

noisy frequency. Figure 14 depicts an example of a noisy frequency signal, with $\omega_s = 1$ Hz and $\sigma_\omega = 2\%$. The bias in the frequency leads to a bias in the phase between the input power signal and the output temperature response. This causes an uncertainty in the phase values, which negatively impacts the ability to accurately recover properties by introducing errors in the recovered properties compared to the true specimen values.

The second type of noise considered is due to a potential phase lag in the radiometric measurements, assumed to be a constant delay inherent to the pyrometer output. One source of this noise can be due to response time characteristics of the device, or the 2-D effects associated with its spot size. However, another noise source can stem from the finite penetration depth of the IR wavelengths into the cross section of the slab.

Considering that the YSZ transparency and emissivity characteristics are a function of wavelength, as well as dependent on the introduction of contaminants over the lifetime of the part [18], it is challenging to quantify the impact of transmittance (which approaches 0% in the 8–11micron range) and bound it with a long wave IR penetration depth. Nevertheless, it would be expected that the manifestation of this phenomena would induce an averaging effect of phase information across the cross-section, which could be considered an additional constant lag to the measurements. However, the exact magnitude associated with this lag remains unknown, without future experimental studies.

Nevertheless, the mathematical representation of the second noise type is modeled by

$$\varphi_n = \varphi_s + \varphi_C \tag{34}$$

$$\varphi_C = \text{Const} \tag{35}$$

where ϕ_s is presumably the real phase representing thermal response, ϕ_C is a constant phase lag bias, and ϕ_n is the actual measured phase with noise. Note that for simplicity we call the phase φ instead of $\delta\phi_3$. The second noise type directly affects the recovery method by introducing bias into the optimization process. In this study, we analyze the error that results from the combination of both noise types. Figure 15 depicts an example of a signal containing a frequency noise with $\omega_s = 1$ Hz and $\sigma_\omega = 2\%$, and phase noise lag $\varphi_C = \pi/6$.

The impact of noise on property recovery is evaluated by introducing prescribed noise into synthetic data inputs based on the two different noise types. In the first type, noise is added to the frequency before phase calculation, and in the second type, noise is

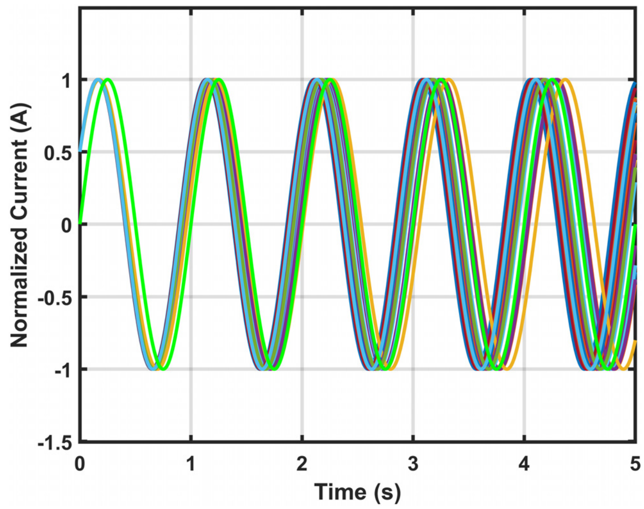

Fig. 15 An exemplary current output signal from the induction coil amplifier with deviations from intended frequency of $\omega_s = 1$ Hz and $\sigma_\omega = 2\%$, and constant phase lag shift of $\varphi_C = \pi/6$, where the ideal signal is depicted in green

added to the phase before the fitting process. The second type of noise is also analyzed using a noisy frequency to evaluate the combined effects of both noise types. This methodology is then repeated for different values of thermal properties and noise levels for both noise types to determine the bounds of error values. The error value of interest is defined as the difference between the specimen's thermal resistance (used to create synthetic data simulations representing actual measured specimens) and the predicted thermal resistance obtained using the recovery methodology with noise.

The probabilistic nature of noise requires repeating the recovery process for high number of iterations, each with a unique combination of frequency and phase error value. To ensure robust results, a total of 200 Monte Carlo simulations (MCSs) are conducted. This generates enough data to accurately capture the stochastic behavior of the system. The converged maximum error is determined through 10 different modulation frequency sweep measurements that form an overdetermined system of equations.

Figure 16 shows the results of the normalized percent error in recovering thermal resistance R for different levels of frequency noise (σ_ω range) and varying number of independent frequency sweep measurement observations.

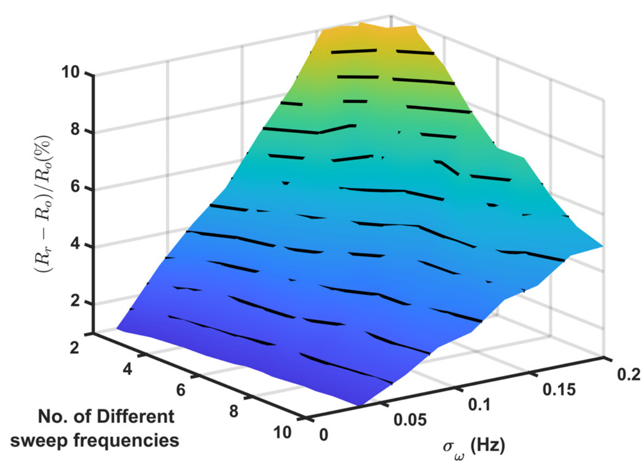

Fig. 16 Normalized percent error in recovery of thermal resistance for range of modulation frequency noise and number of independent frequency sweep observations

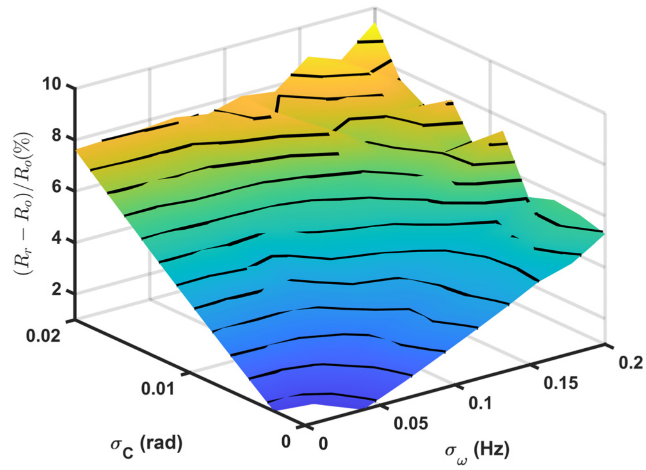

Fig. 17 Normalized percent error in recovery of thermal resistance for range of modulation frequency and phase lag noise levels, while sampling 10 independent frequency sweep observations

For the highest noise level on the modulation frequency 0.2 Hz, even in the worst-case scenario with only two independent frequency sweep measurements, the error in thermal resistance estimation is below 10%. This is a pessimistic estimate for the modulation frequency error, as it has the same order of magnitude as its nominal value. More reasonable levels of frequency deviation (0.05–0.1 Hz) yield thermal resistance recovery within an error range of 2–4%. Moreover, the benefits of increased number of frequency sweep measurements seem to level off at around 10 independent observations, maintaining a thermal resistance estimation error below 5%.

In this light, the impact of additional phase noise at different values is analyzed for 10 independent frequency sweep observations. Figure 17 presents the results of the normalized percentage error in recovering thermal resistance for a combination of frequency and phase noise. The upper bound of phase noise is selected due to the characteristics of commercial pyrometers which generally offer response time in the order of hundreds of microseconds and a frequency in the range of kHz. While a maximum recovery error of 10% is observed in the highest levels of combined noise, more moderate values around 5% are expected for phase lag deviation of 0.05 rad order.

Summary and Conclusions

In this paper, the authors introduce a new method for determining the thermal resistance of thermal barrier coatings (TBCs) using a measure of phase difference between the imposed periodic induction heating and resultant surface radiometry signal. This technique has the advantage of not requiring calibration, as it is independent of the signal strength. The one-dimensional heat transfer problem is solved, assuming that most of the generation occurs near the back of the TBC layer, substantiated by the analysis of Joule heating considerations in Maxwell equations. The temperature input–output across the coating's transfer function is found to depend solely on Biot and Womersley numbers. Then, this expression can be used to determine thermal properties by sweeping the modulation frequency and measuring the relative phase of the surface radiation. Additionally, a simplified expression that depends solely on the thermal Womersley number is deduced, exhibiting validity for conditions typical to TBCs. This nondimensional quantity is shown to be proportional to thermal resistance, taking into account both the thickness (degradation) and the thermal conductivity (increase) effects.

In order to identify the acceptable potential noise levels for the circuit design of a future experimental method demonstration, a synthetic data with varying levels of noise is generated based on the mathematical model, quantifying the error propagation to property recovery. However, this approach cannot account for any small errors that can stem from assumptions or approximations that went into developing the technique and future studies will address this challenge experimentally.

Nevertheless, based on typical values for TBC properties, synthetic data of phase versus frequency is created to numerically test the sensitivity of the method for recovering thermal resistance. Suitable bounds for the frequency sweep range are determined by examining the analytical phase-Womersley relation. The phase output is estimated for a frequency range, and the associated thermal resistance is predicted on a best-fit basis. Comparing the reduced order simplified expression with the full numerical solution that mimics the real-world physics, the method is shown to predict the thermal resistance within a normalized error of 0.8%.

In order to capture experimental conditions, a noise-sensitivity analysis is conducted imposing an uncertainty in modulation frequency, and phase lag. The number of independent frequency sweep observations required to reach estimation error convergence is found to be around 10 for a broad range of conditions. For the worst case of combined noise, a maximum error of 10% in thermal resistance recovery is expected and for more representative noise levels, the resulting error is projected to be around 2–5%.

In conclusion, the described induction phase radiometry is believed to be conducive to in situ monitoring of thin ceramic film thermal resistance in between engine overhauls, considering that the approach is based on: (1) internal heat generation by induction rather than external excitations, (2) relative phase lag difference between the generation and surface temperature response, which is a weak function of external boundary conditions and independent of surface emissivity, (4) low number of required redundant frequency sweep samples to minimize experimental uncertainties, yielding high accuracy estimates resilient to noise. In a future study, the authors intend to demonstrate the technology experimentally, considering that the real engine parts have complex curved geometries, where the relative location and orientation of induction coils may be important. Moreover, the presented framework assumes 1-D conduction and opaque-body radiation, ignoring the multidimensional heat transfer effects whose influence should be quantified in representative conditions.

Funding Data

- European Research Council (ERC) (Grant No 853096; Funder ID: 10.13039/501100000781).

Data Availability Statement

The datasets generated and supporting the findings of this article are obtainable from the corresponding author upon reasonable request.

Nomenclature

A = area of slab
AC = alternating current
A_c = conductor cross-sectional area
B_i = Biot number
c = specific heat capacity
C = heat capacity
CMAS = calcium-magnesium-alumina-silicate
C_p = heat capacity at constant pressure
d = distance from the induction coil to substrate material
E = electrical field
E_0 = electrical field amplitude
$f(t)$ = time dependent surface generation term
f_c = carrier frequency
f_m = modulation frequency
$g(x)$ = heat generation density function
h = convective heat transfer coefficient
H = transfer function
I = current
i = imaginary number $\sqrt{-1}$
I_0 = surface current density
$Im()$ = imaginary component
k = thermal conductivity coefficient
l = conductor length
L = coating Thickness
m = mass
MCS = Monte Carlo Simulation
N() = normal distribution
P = power
PAT = photo-acoustic technique
PopTea = phase of photo thermal emission analysis
PTI-MLA = pulsed thermal imaging multilayer analysis
Q = heat flux
R = thermal resistance
R_0 = prescribed thermal property
$Re()$ = real component
R_{el} = electrical resistance
R_n = thermal resistance heat capacity ratio
R_r = retrieved thermal property
R_s = effective substrate resistance
s = Laplace domain variable
t = time
TBC = thermal barrier coating
TFTCM = thin film thermal conduction meter
T_{sub} = parent material temperature
T_{TBC} = TBC temperature
TWI = thermal wave interferometry
W_o = Womersley number
x = spatial coordinate in thickness plane direction
YSZ = yttria-stabilized zirconia
α = coating thermal diffusivity
δ = penetration depth
ΔT = temperature rise
$\Delta\phi$ = phase error function
$\delta\phi_1$ = electromagnetic field-heat generation phase
$\delta\phi_2$ = heat generation-parent material temperature phase
$\delta\phi_3$ = parent material temperature-TBC temperature phase
μ = magnetic permeability
μ_r = relative permeability
ρ = density
ρ_{el} = electrical resistivity
σ = electrical conductivity
σ_ω = Standard deviation of frequency
ϕ = phase
φ_C = constant phase lag bias
φ_r = reduced expression of phase
φ_s = the presumably real phase
ϕ_Δ = recurring phase in angle domain
ω = angular frequency
$\omega_\cdot$ = probabilistic frequency value
ω_m = angular modulation frequency
ω_n = resulted noisy frequency
ω_s = desired frequency set value
$\mathcal{O}(\,)$ = magnitude of order
$\vec{()}$ = vector term
$\left|\overline{\Delta\phi}\left(\vec{R}\right)\right|$ = absolute average of phase error functions across all frequencies
$\bar{\cdot}$ = term at Laplace domain

Appendix A

Steady State Boundary Conditions Methods. The thin film thermal conduction meter (TFTCM) technique [9] is to determine the thermal conductivity of thin film samples with known thicknesses in the range of 50–1000 μm. The specimen is sandwiched between two thermocouple-instrumented aluminum slabs. All possible loss mechanisms are isolated by performing the experiment in a vacuum within a thermally insulated reflective bell jar. A foil heater located on the bottom slab is used to establish a thermal equilibrium across the material stack through which the thermal conductivity can be determined. Thermal conductivities of four standard thin film materials (Kapton-HN, Kapton-MT, Teflon, and Borofloat glass) are determined within this experimental arrangement. The conductivity values are found to be within a margin of $\pm 5\%$ with respect to the manufacturer's quoted values.

Step Change Boundary Conditions Methods. The laser flash technique is a commonly used method described in the ASTM E1461, that is useful in determining thermal diffusivity over a large range of measurement temperatures [4]. The resulting temperature rise due to laser irradiation is recorded at the rear surface of the sample and is analyzed by comparing it to a mathematical model for a semi-infinite specimen exposed to a pulse of surface heating. The technique is highly sensitive to the uncertainty in the measured coating thickness, with the error increasing as a response to thickness rise, thereby confining meaningful results to thin layers (below 50 μm) [4]. In addition, a $\pm 1\%$ deviation in substrate thickness may affect diffusivity readings by as much as $+60\%/-28\%$ [19]. Measurement accuracy is shown to improve at higher temperatures, where the sensitivity is reduced due to an increased substrate-to-coating conductivity ratio [19]. Considering that the rise time is measured at the back of the specimen and that this method requires a vacuum-inert environment to isolate all other heat exchange mechanisms, this method cannot be applied in situ.

The Pulsed Thermal Imaging Multilayer Analysis (PTI-MLA) is another cutting-edge method that relies on thermal pulse input. It obtains the thermal properties of the TBC from infrared camera images [10]. The method is based on tracking decaying temperature in the surface as it passes through the parent material. Although this scheme is relatively accurate ($<3\%$) and suitable for in situ applications, the IR camera still needs to be calibrated. The temperature-wavelength band correction requires initial calibration at the manufacturer, and a recurring calibration regularly. Additionally, the TBC specimen has to be coated with a high-emissivity material (such as graphite).

Periodic Excitation Boundary Conditions Methods. The 3-Omega technique is closely related to the hot-wire and hot-strip measurements, where a thin metal strip is fabricated on top of the sample using either photolithography or evaporation through a mask [4]. The metal strip is used as both heater and thermometer simultaneously. An AC power source with adjustable frequency is applied to the heater, the temperature response of the element is determined from the heater resistance, and the thermal conductivity is derived from the power and the third harmonic of the temperature or voltage oscillation [4]. This technique is limited to temperatures below 500 °C, since the ratio of the heat radiated from the surface and the heat transported through the solid rises significantly with higher temperatures [4]. Evaluating the accuracy of the 3-Omega method [20], thermal conductivity of a SiO_2 sample is measured along with two standard materials (Pyroceram 9606 glass ceramic and Pyrex 7740 borosilicate glass). The acquired data is compared to the results of an extensive study, despite the large data spread ($\sim 25\%$), a reasonable correlation is found.

The photo-acoustic method is thoroughly studied by Bennett et al. [11], based on the theory described in Ref. [21]. This technique is suggested for acquiring various thermal properties of thin film layers based on the evaluation of a photo-acoustic signal, which is generated at the solid–gas interface of a TBC specimen on a substrate. The surface of the sample is subjected to a frequency-and amplitude-modulated laser beam, resulting in the generation of thermal perturbations within the sample. The interference of these waves affects the amplitude of the thermal response that is transmitted to the gas within the test chamber, which in turn initiates a detectable photo-acoustic response. The photo-acoustic signal is normalized by using the reference signal of a thermally thick layer of the same material to remove the effects of cell resonance and microphone response. The thermal diffusivity of the substrate can be determined from the phase lag between the heat source and the acoustic wave or from the amplitude ratio of the sample and the reference. The phase lag method is confined to thin layers only. According to Xu et al. [4], the signal itself is measured in the frequency range of 100–20,000 Hz, and the technique is limited to a surface temperature rise not exceeding 0.5 K. Experimental complexity limits the technique to a laboratory setting and restrict its applicability to very thin samples with substrates of less than 2.5 mm and TBC layer thickness below 50 μm.

In other works, an alternative approach known as the "phase of photothermal emission analysis" (PopTea) is considered [12]. This method utilizes harmonic laser heating to interrogate the temperature field via the phase of thermal emission from the coating. In a similar manner to the previous method, the phase lag between the input irradiation and output emission measurement is used to derive material thermal properties. In contrast to other methods, PopTea is suitable for measuring the thermal properties of a serviceable engine part at the intermediate or depot level as it only requires access to the front surface of a sample. However, it does not allow measurement in a serviceable engine at the organizational level or at the flight line on wing due to the complexity of required equipment. Furthermore, PopTea facilitates the determination of both thermal diffusivity and effusivity simultaneously by deriving them from the solution to a heat transfer model that produces temporal temperature distribution in the coating combined with a solution of a linear radiation transport model producing emission phase. The time-lag of temperature rise as a response to sample heating is related to the heat transfer length scale (laser penetration depth and TBC thickness) in addition to the thermal diffusivity of the material. Both harmonic heating and concurrent detection are performed from the front surface of the coating by means of laser light and an IR detector, respectively. The phase difference between the laser and the thermal emission is then computed for different heating frequencies. The thickness of the TBC layer needs to be determined in advance by applying another technique. When the coating thickness exceeds certain limits (200 μm), the length scale for transient heat diffusion in the substrate becomes comparable to the laser beam diameter, resulting in the need for a multidimensional heat transfer model. The method relies on a substrate with sufficiently high diffusivity (interface thermal contrast). Comparison with acquired results indicates reasonable agreement within 20%, as the reference laser flash measurements exhibit more than a 15% spread [12].

The thermal wave interferometry (TWI) method resembles the PopTea measurement technique, differing only in the more simplified radiation model implemented, which assumes independence of various parameters as a result of a sensitivity analysis. Thermal 'waves' are partially reflected at the coating-substrate interface and return to produce interference effects at the surface. In reference to an uncoated surface response, the temperature phase variations are recorded, from which the thermal diffusivity and effusivity can be derived. Assessing technique's sensitivity to various factors, it is demonstrated that the acquired phase is more receptive to reflection coefficient than the coating thickness [13]. Compared to laser flash results, the deviations in diffusivity measurements are within a 3–6% margin, while the variance with respect to effusivity ranges from 14–71%. Nevertheless, limitations involving low emissivity coatings preclude the use of this technique on TBC films in situ.

References

[1] Parker, D. W., 1992, "Thermal Barrier Coatings for Gas Turbines, Automotive Engines and Diesel Equipment," Mater Des., **13**(6), pp. 345–351.

[2] Thakare, J. G., Pandey, C., Mahapatra, M. M., and Mulik, R. S., 2021, "Thermal Barrier Coatings—A State of the Art Review," Met. Mater. Int., **27**(7), pp. 1947–1968.

[3] Clarke, D. R., Oechsner, M., and Padture, N. P., 2012, "Thermal-Barrier Coatings for More Efficient Gas-Turbine Engines," MRS Bull., **37**(10), pp. 891–898.
[4] Taylor, R. E., Wang, X., and Xu, X., 1999, "Thermophysical Properties of Thermal Barrier Coatings," Surf. Coat. Technol., **120–121**, pp. 89–95.
[5] Clarke, D., and Phillpot, S., 2005, "Thermal Barrier Coating Materials," Mater. Today, **8**(6), pp. 22–29.
[6] Song, N., Wang, Z., Xing, Y., Zhang, M., Wu, P., Qian, F., Feng, J., Qi, L., Wan, C., and Pan, W., 2019, "Evaluation of Phase Transformation and Mechanical Properties of Metastable Yttria-Stabilized Zirconia by Nanoindentation," Materials, **12**(10), p. 1677.
[7] Swar, R., Hamed, A., Shin, D., Woggon, N., and Miller, R., 2012, "Deterioration of Thermal Barrier Coated Turbine Blades by Erosion," Int. J. Rotating Mach., **2012**, pp. 1–10.
[8] Kakuda, T. R., Levi, C. G., and Bennett, T. D., 2015, "The Thermal Behavior of CMAS-Infiltrated Thermal Barrier Coatings," Surf Coat Technol., **272**, pp. 350–356.
[9] Subramanian, C. S., Amer, T., UpChurch, B. T., Alderfer, D. W., Burkett, C., and Sealey, B., 2006, "New Device and Method for Measuring Thermal Conductivity of Thin-Films," ISA Trans., **45**(3), pp. 313–318.
[10] Sun, J. G., 2014, "Pulsed Thermal Imaging Measurement of Thermal Properties for Thermal Barrier Coatings Based on a Multilayer Heat Transfer Model," ASME J. Heat Mass Transfer-Trans. ASME, **136**(8), p. 081601.
[11] Bennett, C. A., and Patty, R. R., 1982, "Thermal Wave Interferometry: A Potential Application of the Photoacoustic Effect," Appl. Opt., **21**(1), pp. 49–54.
[12] Kakuda, T., Limarga, A., Vaidya, A., Kulkarni, A., and Bennett, T. D., 2010, "Non-Destructive Thermal Property Measurements of an APS TBC on an Intact Turbine Blade," Surf. Coat Technol., **205**(2), pp. 446–451.
[13] Bendada, A., 2002, "Sensitivity of Thermal-Wave Interferometry to Thermal Properties of Coatings: Application to Thermal Barrier Coatings," Meas. Sci. Technol., **13**(12), pp. 1946–1951.
[14] Landau, L., and Lifshitz, E., 1984, *Electrodynamics of Continuous Media*, 2nd ed., Pergamon, Oxford, UK.
[15] Rudnev, V., Loveless, D., and Cook, L. R., 2017, *Handbook of Induction Heating*, 2nd ed., CRC Press, Boca Raton, FL.
[16] Julius, S., Leizeronok, B., and Cukurel, B., 2018, "Nonhomogeneous Dual-Phase-Lag Heat Conduction Problem: Analytical Solution and Select Case Studies," ASME J. Heat Mass Transfer-Trans. ASME, **140**(3), p. 031301.
[17] William, H. H., and John, B. A., 2012, *Engineering Electromagnetics*, 8th ed., McGraw-Hill, New York.
[18] Eldridge, J. I., and Spuckler, C. M., May 2008, "Determination of Scattering and Absorption Coefficients for Plasma-Sprayed Yttria-Stabilized Zirconia Thermal Barrier Coatings," J. Am. Ceram. Soc., **91**(5), pp. 1603–1611.
[19] Taylor, R. E., 1998, "Thermal Conductivity Determinations of Thermal Barrier Coatings," Mater. Sci. Eng.: A, **245**(2), pp. 160–167.
[20] Cahill, D. G., 1990, "Thermal Conductivity Measurement From 30 to 750 K: The 3ω Method," Rev. Sci. Instrum., **61**(2), pp. 802–808.
[21] Rosencwaig, A., and Gersho, A., 1976, "Theory of the Photoacoustic Effect With Solids," J. Appl. Phys., **47**(1), pp. 64–69.